Quantum Electronics **51** (10) 938–946 (2021)

LASER APPLICATIONS AND OTHER TOPICS IN QUANTUM ELECTRONICS https://doi.org/10.1070/QEL17624

Optical detection of an ensemble of C centres in diamond and their coherent control by an ensemble of NV centres

O.R. Rubinas, V.V. Soshenko, S.V. Bolshedvorskii, I.S. Cojocaru, A.I. Zeleneev, V.V. Vorobyov, V.N. Sorokin, V.G. Vins, A.N. Smolyaninov, A.V. Akimov

Abstract. **The nature of decoherence in a diamond plate that is most optimal for magnetometry (i.e., a plate with compromise values of concentration and coherence time of NV centres) is investigated in detail. The concentration of C centres, which serve as donors for the formation of NV centres and at the same time limit their coherence time, is measured in this plate. The ensemble of NV centres in diamond is used as a sensing element, which makes it possible to record the coherence dynamics and concentration of C centres. The recording is performed using the double electron–electron resonance technique. Its significant advantage over IR spectroscopy, which yields some averaged concentration of defects in diamond, is the possibility of measuring locally the concentration of C centres. The method proposed by us yields a value of 50.1 ± 1.4 ppm for the C-centre concentration, which refines the IR spectroscopy data (57.5 ± 4.8 ppm).**

Keywords: *NV centre, C centre, diamond, optically detected magnetic resonance, spin echo, Rabi oscillations, double electron–electron resonance.*

O.R. Rubinas Moscow Institute of Physics and Technology (National Research University), Institutskii per. 9, 141701 Dolgoprudnyi, Moscow region, Russia; Lebedev Physical Institute, Russian Academy of Sciences, Leninsky prosp. 53, 119991 Moscow, Russia; Russian Quantum Centre, ul. Novaya 100A, Skolkovo, 143025 Moscow, Russia; LLC Sensor Spin Technologies, ul. Nobelya 7, Skolkovo, 121205 Moscow, Russia; e-mail: rubinas@phystech.edu;
V.V. Soshenko, S.V. Bolshedvorskii Lebedev Physical Institute, Russian Academy of Sciences, Leninsky prosp. 53, 119991 Moscow, Russia; LLC Sensor Spin Technologies, ul. Nobelya 7, Skolkovo, 121205 Moscow, Russia;
I.S. Cojocaru Lebedev Physical Institute, Russian Academy of Sciences, Leninsky prosp. 53, 119991 Moscow, Russia; Russian Quantum Centre, ul. Novaya 100 A, Skolkovo, 143025 Moscow, Russia;
A.I. Zeleneev Moscow Institute of Physics and Technology (National Research University), Institutskii per. 9, 141701 Dolgoprudnyi, Moscow region, Russia;
V.V. Vorobyov The University of Stuttgart, Keplerstraβe 7, Stuttgart, 70049 Germany;
V.N. Sorokin Lebedev Physical Institute, Russian Academy of Sciences, Leninsky prosp. 53, 119991 Moscow, Russia; Moscow Institute of Physics and Technology (National Research University), Institutskii per. 9, 141701 Dolgoprudnyi, Moscow region, Russia;
V.G. Vins LLC Velman, ul. Zelenaya Gorka 1/3, 630060 Novosibirsk, Russia;
A.N. Smolyaninov LLC Sensor Spin Technologies, ul. Nobelya 7, Skolkovo, 121205 Moscow, Russia;
A.V. Akimov Texas A&M University, 4242 TAMU, College Station, USA; LLC Sensor Spin Technologies, ul. Nobelya 7, Skolkovo, 121205 Moscow, Russia; Russian Quantum Centre, ul. Novaya 100 A, Skolkovo, 143025 Moscow, Russia

Received 3 June 2021
Kvantovaya Elektronika **51** (10) 938–946 (2021)
Translated by Yu.P. Sin'kov

1. Introduction

The NV centre in diamond [1] is one of the most important lattice defects, which is applied in various fields of science. The structure of this centre in the diamond lattice is shown in Fig. 1a. NV centres in diamond are often used to detect magnetic and electric fields. Impressive results have been obtained in different versions of magnetometry, such as magnetometry of high spatial resolution [2], detection of weak magnetic fields [3], magnetic scanning in biological objects [4], magnetic resonance tomography (MRT) [5], and detection of external spins [6].

Concerning the use in high-precision magnetometry, one of the best (known to date) samples are diamond plates grown at high temperature and pressure, having a concentration of nitrogen-containing defects of ~80 ppm, including the concentration of NV centres of ~14 ppm [7]. To gain a deeper insight into the limitations of the magnetic sensitivity of these plates, it is necessary to develop methods for measuring paramagnetic impurities that limit the coherence time of NV centres. Previously paramagnetic defects were studied by IR spectroscopy [7–9], which makes it possible to detect a wide class of defects but has significant limitations on the accuracy and absolute calibration of measurements.

An ensemble of NV centres can also be used to detect external spins. One of the methods implementing this approach is the technique of double electron–electron resonance (DEER) [10], in which the influence of external spin field on an ensemble of NV centres is used. The DEER technique is generally based on the classical electron spin resonance (ESR). In this study we applied the optical version of DEER, based on the properties of optically recorded state of NV centres, interacting with C centres, whose state is not detected optically. The C centre (which is also often referred to as p1 centre) is a donor nitrogen atom replacing a carbon atom in diamond. Figure 1b shows the structure of C centre in the diamond lattice.

The possibility of applying NV centres as sensors of spin defect field in diamond is closely related to the intrinsic properties of NV centres. The latter are luminescent defects in diamond, which make it possible to detect optically the state of their electron spin. Moreover, the NV-centre state can be controlled using a combination of electromagnetic fields in the optical and microwave ranges [11]. The implementation of DEER on NV centres in diamond is based on the use of the so-called spin echo sequence [12]. A spin echo signal is sensitive to ac magnetic fields when their half period coincides with the echo sequence period. Since the spins of C centres in diamond, which precess in an external dc magnetic field, form a field alternating in time, these centres can be detected by their influence on the spin echo signal from NV centre [13].

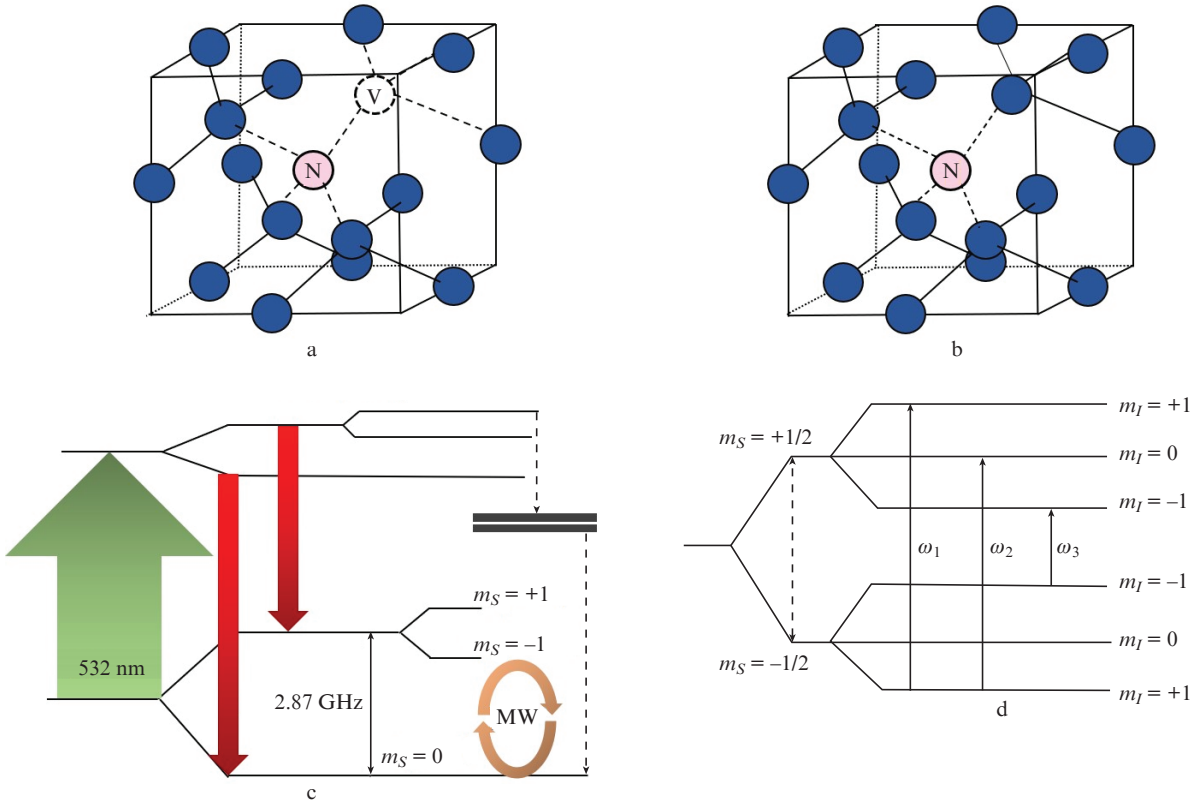

Figure 1. (Colour online) (a) Position of an NV centre in the diamond lattice: one carbon atom is replaced with a nitrogen (N) atom, and one of its neighbors is absent (V); (b) position of a C centre in the diamond lattice: one carbon atom is replaced with a nitrogen atom; (c) energy-level diagram for the NV centre in an external dc magnetic field: semicircular arrows show the transitions controlled by microwave field, the solid arrow (2.87 GHz) is the splitting of NV-centre sublevels in the zero magnetic field, the green arrow is the laser pumping of upper energy levels, the red arrows are radiative transitions from the excited to the ground state, and dashed arrows are nonradiative transitions to the ground state with zero electron spin projection; (d) energy-level diagram for the C centre in an external dc magnetic field: the dashed arrow is the Zeeman splitting, m_S and m_I are the projections of the electron and nuclear spins of C centre, and the solid arrows indicate allowed transitions with frequencies of ω_1, ω_2, and ω_3.

The use of NV centre as a magnetic field sensor is directly related to its spin properties: the coherence time and the width of the so-called optically detected magnetic resonance (ODMR) [14]. The coherent properties of NV centre are determined to a great extent by its environment: electron and nuclear spins existing present in diamond. Many of spin possessing defects do not luminesce under normal conditions; they are considered as 'dark' or 'nonradiative'. One of the main impurities in diamond is C centre; it belongs to the most widespread defects in this material, whose presence is necessary for the formation of NV centres.

C centres, which have an electron spin $S = 1/2$, form the so-called electron spin bath [15]; this bath, containing NV centres, affects their coherence. To date, direct influence of the C-centre concentration on the coherence time of NV centres has been demonstrated [14]; this influence manifests itself in a significant decrease in the attainable sensitivity of the magnetic field sensor based on NV centres. A possible way to solve this problem is to reduce the total nitrogen concentration in diamond; however, the concentration of useful NV centres will drop as well [16]. Thus, it is necessary to reduce the concentration of C centres with respect to NV centres. In this case, a problem of simultaneous measurement of the C-centre concentration arises.

It is generally accepted to measure the concentration of C centres in diamond using one of two methods: ESR spectroscopy [17] or IR spectroscopy [9]. However, they both are applicable only when the total number of defects in a sample is large, whereas a possibility of carrying out measurements in relatively small diamond samples with a low concentration of defects and, correspondingly, their small total number is important for many applications. Of interest is also the possibility of on-line concentration measurements, without application of many various devices. In this study we demonstrate experimentally the possibility of measuring the concentration of C centres using an ensemble of NV centres.

2. Results

2.1. Fundamentals of the optical reading of the NV-centre state

As was mentioned above, the spin echo signal on an NV-centre ensemble is sensitive to the ac magnetic fields induced on it. The ground state of the NV centre (Fig. 1c) has a total electron spin $S = 1$; it is split in a dc magnetic field to form a triplet. The natural quantisation axis for NV-centre states is the axis connecting the nitrogen atom with the vacancy. The electron spin projections on this axis are good quantum numbers. Being exposed to 532-nm laser radiation, an NV centre is partially polarised to a state with a spin projection $m_S = 0$ [1] due to the presence of metastable singlet levels, through which nonradiative decay of an excited state of the NV centre to the ground state with an electron spin projection $m_S = 0$ occurs. A weak external magnetic field (~10 G) causes a sufficiently large (2.8 MHz G^{-1}) splitting of states with electron spin projections $m_S = +1$ and –1 on the axis of the NV centre,

which makes it possible to manipulate pairs with projections of 0, –1, and +1 as two-level systems. The $|m_S = 0\rangle \leftrightarrow |m_S = -1\rangle$ transition was used in this study. The echo sequence [12] for NV centres is a sequence of microwave pulses with a period $\pi/2 - \tau - \pi - \tau - \pi/2$ at the resonance frequency of the $|m_S = 0\rangle \leftrightarrow |m_S = -1\rangle$ transition of the ground state of the NV centre, which are applied after polarizing the electronic state $|m_S = 0\rangle$. The first ($\pi/2$) pulse in the echo sequence transfers the NV centre to the superposition state $(1/\sqrt{2})|m_S = 0\rangle + (1/\sqrt{2})|m_S = -1\rangle$, whose phase is sensitive to magnetic field and is accumulated for a time τ. After applying the π pulse, the direction of electron spin precession in NV centres in the superposition state changes to opposite, due to which the influence of dc fields on the phase of this state can be eliminated. However, the phase of an ac magnetic field, whose half-period coincides with the echo sequence period, will shift by half period, and its influence will not be excluded. Thus, the echo sequence can be considered as a peculiar lock-in detector for an ac magnetic field. Free precession of C-centre spins, being asynchronous, forms a random field on an NV centre. At the same time, if the spins of C centres are controlled [by applying a resonance RF field (Fig. 1d) at the frequency of the $|m_S = -1/2\rangle \leftrightarrow |m_S = +1/2\rangle$ transition], the field of these spins on the NV centre will be coherent, and its influence can be measured.

2.2. Experimental setup

A schematic of the experimental setup is presented in Fig. 2a. The radiation source is a laser generating at a wavelength of 532 nm (Compass, Coherent Inc.). An acousto-optic modulator (AOM) is used to control the laser beam by switching it off during manipulations with the electron spin state. The laser beam is focused by a collecting lens with a focal length of 3.5 cm on a diamond sample surface into a focal spot with a radius of ~7.5 μm. The laser power in front of the sample is 43 mW. The fluorescence signal of NV centres, collected by a system composed of two parabolic concentrators, is transmitted to a photodetector through a filter transparent for wavelengths above 650 nm.

The system for controlling the electron spin states of the defects under consideration consists of two parts: a microwave part (MW in Fig. 2a) for controlling the state of NV centres and an RF part (RF in Fig. 2a) for controlling the states of C centres. Each part contains a generator; a controlled key, connected to a pulse-generating board; and a pulse amplifier, operating in the corresponding frequency range. The outputs of both amplifiers are connected to a frequency mixer, which transfers the signal to an antenna, inside which a sample is located. The antenna consists of one turn with a diameter of ~5 mm. The diamond sample is oriented in the antenna so that the crystallographic axis [111] of diamond is perpendicular to the turn axis.

We used diamond with a high initial concentration of donor nitrogen (~80 ppm), grown by the HPHT method [9] and irradiated by an electron beam having a density of 15×10^{17} cm^{-2}, with subsequent annealing at 800 °C to form NV centres [9]. Splitting of magnetic sublevels $|m_S = -1\rangle$ and $|m_S = +1\rangle$ is provided by a permanent magnet, oriented so as to make the magnetic field direction (which is quantisation axis for colour centres) coincide with the direction of crystallographic axis [111] in diamond plate.

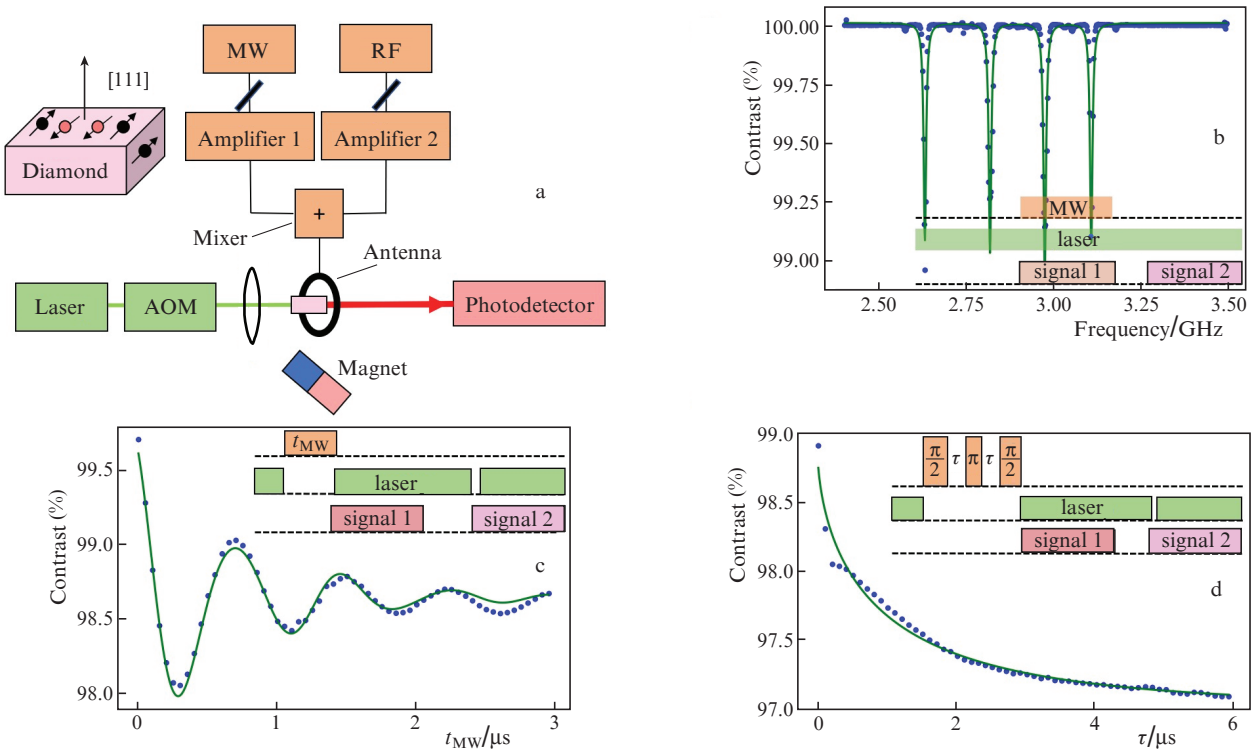

Figure 2. (Colour online) (a) Schematic of the setup: the crystallographic axis [111] is oriented parallel to the dc magnetic field direction, (b) spectrum of ODMR signal from an NV centre in diamond, (c) Rabi oscillations of NV centre, and (d) spin echo signal from an NV centre. In panels b–d the ratio of signal 1 (measured by photodetector) to signal 2 (contrast) is plotted on the ordinate axis; pulses used to control the states of the NV-centre ensemble and detect them are also schematically presented (circles are experimental data and solid lines are the approximation result).

2.3. Method for detecting impurities

To determine the resonance frequency of the $|m_S = 0\rangle \rightarrow |m_S = -1\rangle$transition, which is necessary to implement an echo sequence on an NV centre, we measured the ODMR signal spectrum (Fig. 2b) [18]. The axes of NV centres can be oriented in the diamond lattice along four possible directions, one of which coincides with the [111] axis and, therefore, with the magnetic field direction. The projection of the magnetic field on the lattice axis coaxial with it is maximum, and the projections on the three remaining directions are identical in view of the crystal symmetry. Maximum splittings of degenerate magnetic sublevels $|m_S = -1\rangle$ and $|m_S = +1\rangle$ (specifically, frequencies of 2.63 and 3.11 GHz) correspond to the ensemble of NV centres oriented coaxially with the magnetic field direction. The ensemble of NV centres oriented along the three misaligned directions is characterised by smaller sublevel splittings (specifically, frequencies of 2.82 and 2.97 GHz) because of the smaller magnetic field projection. In this study, the carrier frequency of π pulses was taken to be the central resonance frequency: 2.63 GHz. In addition, the magnetic field B applied to the diamond sample was determined based on the measured frequency:

$$B = \frac{f_{m_S=+1} - f_{m_S=-1}}{2\gamma} = 85 \pm 3 \text{ G}, \quad (1)$$

where $\gamma = 2.8$ MHz G^{-1} is the gyromagnetic ratio and $f_{m_S=\pm1}$ are the frequencies corresponding to two projections of the electron spin of NV centres oriented coaxially with the magnetic field.

The duration of the π pulse for the $|m_S = 0\rangle \rightarrow |m_S = -1\rangle$ transition was calculated proceeding from the frequency of Rabi oscillations (Fig. 2c), which were measured at the frequency determined previously. To this end, an ensemble of NV centres was initialised to the $|m_S = 0\rangle$ state using a laser pulse, after which a microwave pulse arrived and then another laser pulse, during which the NV-centre luminescence signal was read (signal 1 in Fig. 2). The resulting signal is shown in Fig. 2c. Here, the intensity of the centre luminescence signal in the absence of microwave pulse (signal 2 in Fig. 2) was taken to be 100%. The duration of the π pulse was determined from the measured oscillation period to be 300 ns at a microwave field power of 15.8 W at the mixer output.

The similarly obtained luminescence signal of the NV centre after applying the echo sequence $\pi/2 - \tau - \pi - \tau - \pi/2$ is shown in Fig. 2d as a function of the time τ of electron spin free precession. It can be seen that the spin echo signal is a decaying curve. According to [12], the shape of this signal is described by the expression

$$F_{\text{echo}} = \alpha e^{-(2\tau/T_2)^{\varkappa}}, \quad (2)$$

where α, $\varkappa$, and T_2 (the coherence time of the NV-centre ensemble) are the parameters of the modelling function.

The spectrum of C centres was measured using the pulse sequence presented in Fig. 3c. An RF field in the frequency range of 100–500 MHz was applied at the midpoint of the NV-centre echo sequence. This range covers all expected frequencies of C-centre splitting. Thus, we obtained optical DEER spectra for the C centre (see Figs 3a and 3b).

The energy levels of the ground state of C centre are split in the applied magnetic field B. Their hyperfine structure must be taken into account. The spin Hamiltonian of the C centre can be written as

$$H_C = \mu_B \boldsymbol{B} g \boldsymbol{S} + \mu_I \boldsymbol{B} \boldsymbol{I} + \hbar \boldsymbol{S} A \boldsymbol{I} + \hbar \boldsymbol{I} Q \boldsymbol{I}, \quad (3)$$

where μ_B is the Bohr magneton; μ_I is the magnetic moment of nitrogen nucleus; g, A, and Q are the tensors of the g factor, hyperfine interaction, and quadrupole interactions, respectively; and $\boldsymbol{I}$ is the nitrogen nuclear spin.

The nitrogen nuclear spin $I = 1$ has three possible projections, $\mu_I = -1$, 0, and +1, whereas the electron spin $S = 1/2$ has two projections: $m_S = -1/2$ and +1/2. Thus, the C centre has

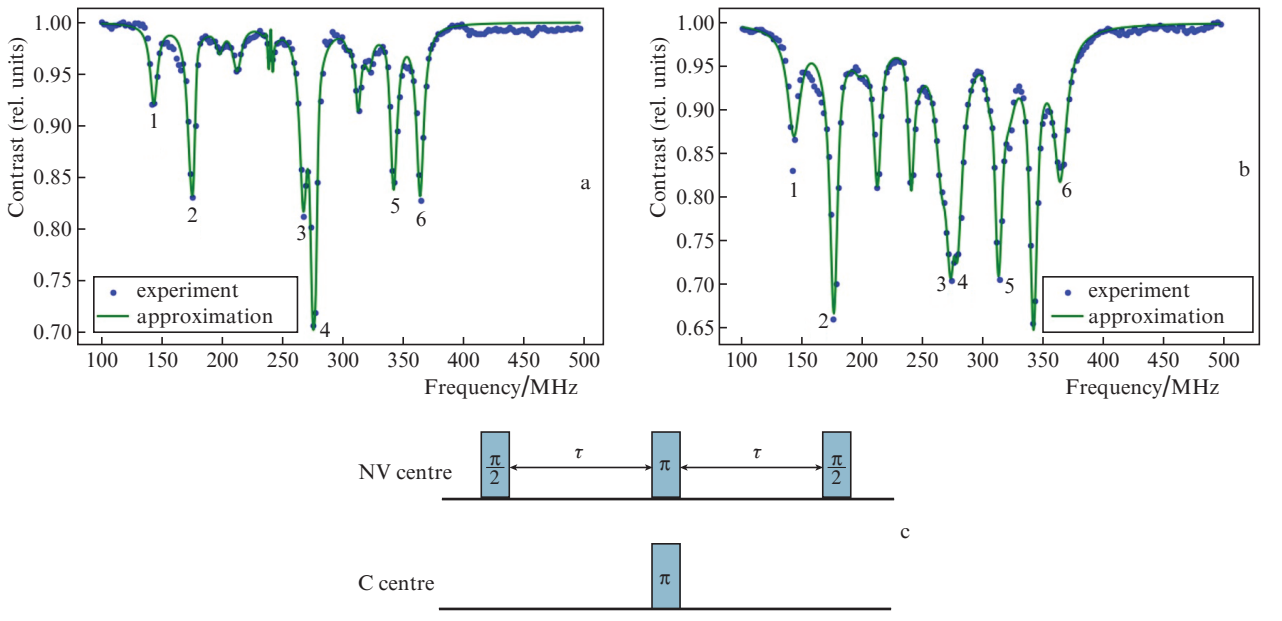

Figure 3. Optical DEER spectra of an ensemble of C centres in diamond at RF powers of (a) 100 and (b) 1000 mW, obtained by applying sequences of pulses (c). The time $\tau = 2$ μs in the echo sequence for the NV centre is fixed, the frequency of the RF pulse acting on the C centre is varied, and the π pulse duration is 300 ns; 1 to 6 are the resonance numbers.

two electron levels, which are split into three hyperfine components (Fig. 1d). Three transitions, retaining the nitrogen nuclear spin, are allowed between these levels in the dipole approximation:

$$|m_S = -1/2, m_I = 0\rangle \leftrightarrow |m_S = +1/2, m_I = 0\rangle,$$
$$|m_S = -1/2, m_I = -1\rangle \leftrightarrow |m_S = +1/2, m_I = -1\rangle, \quad (4)$$
$$|m_S = -1/2, m_I = +1\rangle \leftrightarrow |m_S = +1/2, m_I = +1\rangle.$$

The C centre in diamond has the same symmetry as the NV centre, and, due to the Jahn–Teller effect [19], there are four isolated orientations of C-centre axes in diamond. Thus, in the general case, the spectrum of the C centre should exhibit 12 transitions, that is, four sets of transitions, presented in (4). In a magnetic field coaxial with one of the diamond crystallographic axes (the [111] axis in our case), there are two isolated orientations for C centres: with axes oriented along the magnetic field and with axes oriented along other three possible directions, symmetric relative to the [111] axis. Since each of these two orientations is characterised by their own transition frequency (4), the resonance spectrum of the C centre exhibits six allowed transitions: three for the coaxial orientation and three for other symmetric misaligned orientations. At a magnetic field on the order of 80 G the transitions corresponding to the level with $m_I = 0$ have closely spaced resonances in the DEER spectrum of the C centre for both groups (Fig. 3a). It should be noted that, along with the transitions presented in (4), the spectrum contains also transitions corresponding to a change in the nitrogen nuclear spin by unity, specifically:

$$|m_S = -1/2, m_I = 0\rangle \leftrightarrow |m_S = +1/2, m_I = -1\rangle,$$
$$|m_S = -1/2, m_I = -1\rangle \leftrightarrow |m_S = +1/2, m_I = 0\rangle, \quad (5)$$
$$|m_S = -1/2, m_I = +1\rangle \leftrightarrow |m_S = +1/2, m_I = 0\rangle,$$
$$|m_S = -1/2, m_I = 0\rangle \leftrightarrow |m_S = +1/2, m_I = +1\rangle.$$

The intensities of the corresponding spectral lines of forbidden transitions (5) significantly increase with an increase in the RF field power (Fig. 3b). A change in the relative line amplitudes for the allowed transitions (4) is also observed, which is indicative of different saturation intensities for different transitions.

To determine the line positions, the DEER spectrum presented in Fig. 3a was approximated by the function

$$f(\omega) = 1 - \sum_{i=1}^{N} C_i \frac{\Gamma^2}{(\omega - \omega_i)^2 + \Gamma^2}, \quad (6)$$

where Γ is the profile half-width; N is the number of resonances; C_i is the ith-resonance amplitude; and ω_i is the central frequency of the ith transition, obtained by solving the time-independent Schrödinger equation with the Hamiltonian (3) for the transitions (4) and (5). The peak amplitudes were assumed to be free parameters in view of the aforementioned effect of line amplitude saturation at different RF field powers. Note that line amplitudes can also be reduced by choosing the RF pulse amplitude and duration for each of the observed transitions such as to make them correspond to the π pulses of the corresponding transition within the ground state of the C centre. Under these conditions, the signal contrast is maximum; it is determined by only the C-centre orientation (see Appendix 1).

By analogy with the obtained Rabi oscillations for NV centres, we found population oscillations for the states responsible for each of the demonstrated allowed transitions, corresponding to the DEER frequencies. To this end, the RF frequency was tuned to the frequency of the corresponding transition (1–6 in Fig. 3a), the RF power was fixed, and the pulse duration was varied (Fig. 4a). The detected signal was the fluorescence signal of NV centres after applying the aforementioned sequence of microwave pulses with a fixed time τ = 2 μs in the echo sequence for the NV centre (Fig. 4b). The amplitude of this signal depends on the magnetic field induced

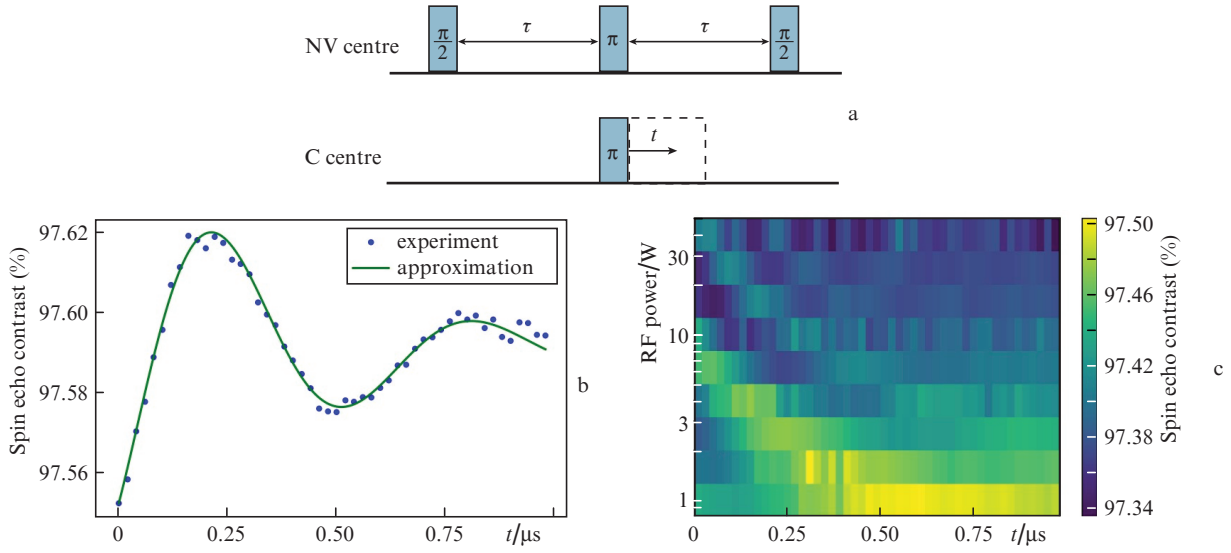

Figure 4. (Colour online) (a) Sequence of pulses at resonance frequencies of transitions 1–6 in Fig. 3a for controlling the C-centre states (the time τ = 2 μs in the echo sequence for NV centre is fixed, the RF pulse duration t is varied in the range of 110–1000 ns, and the π pulse duration is 300 ns); (b) oscillations of level populations (spin echo contrast) for resonance transition 1 in Fig. 3a, obtained with a sequence of pulses presented in panel a; (c) dependence of the oscillations of level populations for transition 1 (Fig. 3a) in a C centre on the RF pulse power.

by the C centre and, correspondingly, on the populations of C-centre levels. Thus, optical detection of Rabi oscillations between the levels of C centres is performed.

The oscillations presented in Fig. 4b were approximated by the function

$$f(t) = a + C\cos(2\Omega t + \varphi)e^{(-t/T_2)}, \quad (7)$$

where a, C, Ω, T_2, and φ are the function parameters. The oscillation period $(2\Omega)^{-1}$ of the function $f(t)$ is equal to doubled π-pulse duration.

The Rabi oscillation frequency for C centres and, therefore, the π-pulse duration for C centres depend on the RF field power, as is shown in Fig. 4b. Further measurements were performed with an RF field power chosen so as to make the π-pulse duration the same for C and NV centres. This operation was repeated for each allowed transition, and thus we obtained the power values listed in Table 1.

Table 1. RF field powers at the mixer output, P_{RF}, at which a 300-ns RF pulse serves a π pulse for each transition.

Transition	P_{RF}/W	Transition	P_{RF}/W
1	1.6	4	0.8
2	2.5	5	2.5
3	0.8	6	0.6

To determine the C-centre concentration, we applied a pulsed DEER sequence with varying time t before applying an RF π pulse (Fig. 5a). The pump pulse at an instant t inverts the spins of C centres, thus changing the local field on NV centres, which is caused by the electron–electron interaction, with an energy corresponding to the frequency [20]

$$\omega_{ee} = \frac{\mu_0\gamma^2\hbar^2}{4\pi}\frac{1}{r_{AB}^3}(3\cos^2\theta_{AB} - 1) + J, \quad (8)$$

where r_{AB} is the distance between two interacting centres; θ_{AB} is the angle between the directions of dc magnetic field and the radius vector connecting a pair of NV and C centres; $\mu_0 = 4\pi \times 10^{-7}$ H m^{-1} is the magnetic constant; and J is the frequency corresponding to the exchange interaction energy.

As a result of the electron–electron interaction between NV and C centres at the instant of spin echo formation, an ensemble of NV centres acquires an additional phase $\Delta\varphi = \omega_{ee}t$ [20]. Thus, the frequency ω_{ee} ω_{ee} can be determined by observing the spin echo amplitude as a function of time t. Since the sequence duration is fixed, the change in the echo-signal amplitude is not affected by the transverse relaxation. The spin echo amplitude for each isolated pair of centres changes according to the law $V \propto \cos(\omega_{ee}t)$ [20]. For an ensemble of C and NV centres, it is necessary to perform averaging over this ensemble. This procedure was carried out in [20] for the case of uniform distribution of C centres in diamond, with exchange interaction disregarded; it yielded

$$V(t) \propto e^{-knF_Bt} = e^{-t/T_D}, \qquad k = \frac{2\pi\mu_0\mu_B^2 g_C g_{NV}}{9\sqrt{3}\hbar}, \quad (9)$$

where n is the concentration of C centres in the sample; F_B is the fraction of C centres excited by RF π pulse; t is the application time of RF π pulse for a C centre in the sequence in Fig. 5a; g_C is the g factor of C centre; g_{NV} is the g factor of NV

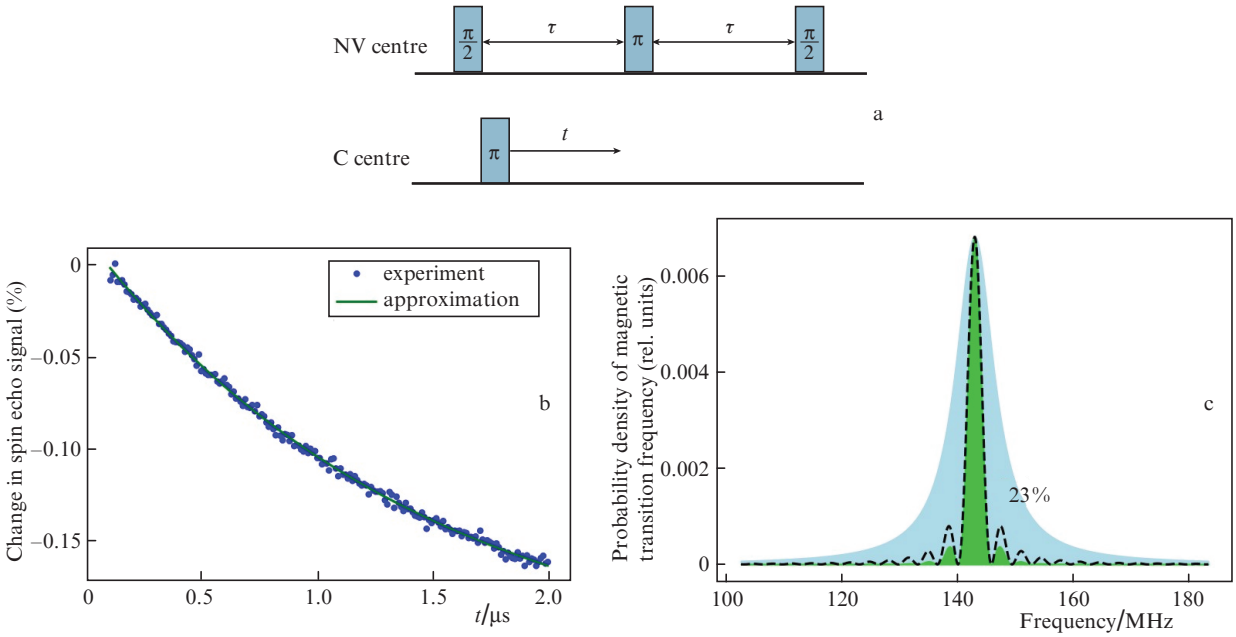

Figure 5. (Colour online) (a) Sequence of pulses for controlling spin flip in C centres by applying a π pulse at a specified instant t on the interval from 0 to τ: the time $\tau = 2$ μs in the echo-sequence for NV centres is fixed, and the sequence is applied for each resonance transition separately; (b) signal attenuation as a result of application of a sequence presented in panel (a) in dependence of the application instant; (c) probability density of magnetic transition frequency for a C centre: (blue colour) homogeneously broadened (Lorentzian) line of the transitions under consideration, (dashed line) probability of implementing a transition at a specified frequency in a C centre after applying an RF π pulse, and (green colour) distribution of the C centres that underwent a transition at the specified frequency after applying an RF π pulse; this example corresponds to the first resonance transition, for which the fraction of excited C centres amounted to about 23%.

centre; and $T_D = 1/(knF_B)$ is the parameter obtained from the experimental data presented in Fig. 5b.

To determine the concentration n, one must know also the coefficient F_B. The fraction of C centres excited by RF π pulse is found as follows [20]:

$$F_B = \int_{-\infty}^{\infty} \frac{\Omega^2}{\Omega^2 + (x-\omega_{RF})^2} \sin^2\left(\sqrt{\Omega^2 + (x-\omega_{RF})^2}\frac{t_p}{2}\right) L(x)\,dx, \quad (10)$$

$$L(x) = \frac{1}{\pi}\frac{\Delta\omega}{\Delta\omega^2 + (\omega-\omega_{RF})^2},$$

where Ω is the oscillation frequency for the population of C-centre levels; ω_{RF} is the resonance frequency for each of the six transitions related to the C centre (affected by π pulse); t_p is the π-pulse duration; $L(x)$ is the transition line profile; and $\Delta\omega$ is the half-width of the line profile at DEER half maximum (Fig. 3a).

We obtained the values of F_B function by numerical calculation of the integral in (10) for each individual resonance frequency of transitions 1–6 in the spectrum in Fig. 3a. The Ω, t_p, and ω_{RF} values were taken to be the above-determined values of Rabi frequencies, π-pulse duration, and each resonance frequency. The $\Delta\omega$ value was also found individually for each resonance from the DEER spectrum obtained by applying a π pulse (see Appendix 1).

The concentration of C centres was calculated for each allowed resonance from the formula

$$n_i = \frac{1}{kT_D F_B},\ i = 1, \ldots, 6. \quad (11)$$

As was discussed above, each allowed resonance corresponds to a certain orientation of C centres with respect to the [111] axis and a certain projection of nitrogen nuclear spin on the centre axis. Therefore, the total concentration n_{tot} was found as the sum of the concentrations corresponding to each resonance:

$$n_{tot} = \sum_{i=1}^{6} n_i, \quad (12)$$

It turned out to be 50.1 ± 1.4 ppm, a value close to the measured concentration of C centres in this diamond plate by IR spectroscopy, 57.5 ± 4.8 ppm (see Appendix 2), within the experimental error (see Appendix 3).

3. Conclusions

In this study we refined the concentration of C centres in a diamond plate that is interesting for magnetometry due to its optimal relationship between the ODMR contrast and linewidth. An ensemble of NV centres was used as a highly sensitive sensor, which makes it possible to record coherent dynamics and concentration of C centres in this plate. Detection was performed using optical DEER, which allowed us to determine the concentration of C centres: 50.1 ± 1.4 ppm, a result refining the IR spectroscopy data: 57.5 ± 4.8 ppm. Note that the method in use makes it possible to measure concentration locally, whereas IR spectroscopy yields only a value averaged over the entire diamond volume. Since C centres are one of the main sources of decoherence of NV centres, the possibility of measuring directly their concentration and controlling the state of C-centre ensemble is an important step in the investigations aimed at designing sensors based of NV centres in diamond.

Appendix 1. DEER spectrum recorded with the aid of individual π pulses

To determine the 'true' amplitude ratios for allowed DEER lines, we recorded spectra in the vicinity of each resonance, using the corresponding π pulses for each of them. An example of these spectra is presented in Fig. 1A.1. A spectrum constructed based on formula (6) is also shown for comparison. The resonance positions in formula (6) were calculated from formula (3) using the Python package QuTiP. The magnetic field in the calculation was assumed to be coaxial with the [111] crystallographic axis and equal to 85 G. As in [14], the coefficients C_i in formula (6) were taken to be 1/12 for all transitions. The half-width Γ of the resonance in (6) was chosen as the average of resonance half-widths: 3.65 MHz. It can be seen that the amplitude ratios for the experimental spectra do not coincide with the theoretical estimate but behave similarly. The discrepancy may be due to the assumption of equal amplitudes for all resonances, which, however, was not analysed in detail in this study.

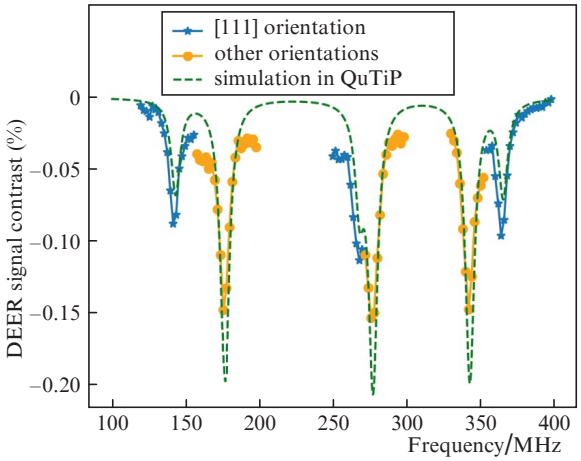

Figure 1A.1. (Colour online) DEER spectrum of all allowed transitions in a C centre, obtained by applying π pulses corresponding to each of the six resonances: (blue) resonance triplet for the ensemble coaxial with the [111] orientation, (yellow) triplet of three other ensembles, and (dashed green line) envelope of all simulated resonances on twelve allowed transitions.

Appendix 2. Check measurement of the C-centre concentration in the sample

The IR absorption spectrum of the diamond plate under study is shown in Fig. 1A.2.

The concentration of C centres is related to the absorption coefficient μ_{1130} at the maximum of the C-centre absorption band by the expression [9]

$$n = (25 \pm 2)\mu_{1130}, \quad (A2.1)$$

where the factor 25 ± 2 ppm cm was obtained experimentally in [9]. Along with the aforementioned error, the spectrum noisiness was taken into account; its contribution to the total

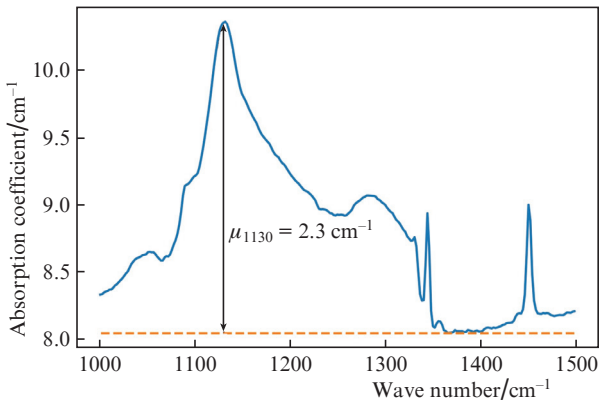

Figure 1A.2. (Colour online) IR absorption spectrum of the diamond plate under study. The dashed line corresponds to the absorption coefficient of this plate free of impurities.

error was found to be 0.16 ppm. Thus, the calculated concentration of C centres in the sample studied was $n = 57.5 \pm 4.8$ ppm.

Appendix 3. Estimation of errors in calculating the concentration

The C-centre concentration n is calculated from the damping approximation according to formula (11); it depends on the damping parameter T_D of the DEER signal and the calculated fraction of C centres excited by the RF field, F_B. Based on this, the error in determining the C-centre concentration n_{tot} can be estimated as the error of the complex function

$$\delta n_{tot} = \sqrt{\sum_{i=1}^{6} \delta n_i^2}\,,$$
$$\delta n_i = \sqrt{\left(\frac{\partial n_i}{\partial T_D}\delta T_{Di}\right)^2 + \left(\frac{\partial n_i}{\partial F_{Bi}}\delta F_{Bi}\right)^2}\,. \qquad \text{(A3.1)}$$

Here, the subscript i enumerates the values related to the ith allowed resonance. The δT_D value was estimated as the error in approximating the DEER signal damping by the least-squares method; it is listed in Table 2 for each of the six resonances. The fraction of C centres excited by the RF field, F_B, is also a complex function of the parameters ω_i, $\Delta\omega_i$, Ω_i [see formula (10)]. However, it can easily be shown that

$$\frac{\partial F_{Bi}}{\partial \omega_i} = 0, \quad \frac{\partial F_{Bi}}{\partial \Omega_i} = 0. \qquad \text{(A3.2)}$$

Therefore, the main contribution to the error in determining F_{Bi} is made by the error in determining $\Delta\omega_i$. Hence, of importance are the second-order errors, which were calculated using the general formula of standard deviation:

$$\delta F_{B\Omega i} = \sqrt{\langle F_{Bi/\Omega}^2\rangle - \langle F_{Bi/\Omega}\rangle^2}\,,$$
$$\delta F_{B\omega i} = \sqrt{\langle F_{Bi/\omega}^2\rangle - \langle F_{Bi/\omega}\rangle^2}\,, \qquad \text{(A3.3)}$$
$$\delta F_{B\Delta\omega i} = \sqrt{\langle F_{Bi/\Delta\omega}^2\rangle - \langle F_{Bi/\Delta\omega}\rangle^2}\,,$$

where $\langle F_{Bi}\rangle_\Omega$, $\langle F_{Bi}\rangle_\omega$, and $\langle F_{Bi}\rangle_{\Delta\omega}$ indicate averaging over Ω_i, ω_i, and $\Delta\omega_i$ respectively. Assuming the Ω_i, ω_i, and $\Delta\omega_i$ values to be normally distributed according to the law

$$N_0(x) = \frac{1}{\sigma\sqrt{2\pi}}\exp\left[-\frac{1}{2}\left(\frac{x - x_{av}}{\sigma}\right)^2\right], \qquad \text{(A3.4)}$$

where x_{av} and σ, respectively, the mean and the standard deviation of the corresponding value, we obtain standard formulas for calculating the mean:

$$\langle F_{Bi}\rangle_h = \int F_{Bi} N_0(x)\,dh\,,$$
$$\langle F_{Bi}^2\rangle_h = \int F_{Bi}^2 N_0(x)\,dh\,, \qquad \text{(A3.5)}$$
$$h = \Omega_i, \omega_i, \Delta\omega_i.$$

The means of the parameters Ω_i, ω_i, $\Delta\omega_i$ and their standard deviations were taken to be the values of the corresponding parameters in the function approximating experimental data and their approximation errors. The resonance obtained by applying an RF π pulse was used for $\Delta\omega_i$. Thus, the total error in determining F_{Bi} for each allowed resonance was

$$\delta F_{Bi} = \sqrt{\delta F_{B\Omega i}^2 + \delta F_{B\omega i}^2 + \delta F_{B\Delta\omega i}^2}\,, \qquad \text{(A3.6)}$$

Table 2. Errors of measured parameters.

Error	Resonance number					
	1	2	3	4	5	6
$\lvert\partial F_{Bi}/\partial\Delta\omega_i\rvert$/MHz^{-1}	0.005	0.012	0	0	0.003	0.002
$\delta\omega_i$/MHz	0.33	0.21	0.27	0.12	0.26	0.20
$\delta\Omega_i$/MHz	0.02	0.02	0.04	0.01	0.06	0.03
$\delta\Delta\omega_i$/MHz	0.54	0.27	0.75	0.36	0.79	0.39
$\delta F_{B\Omega i}$	0	0.001	0.002	0	0.003	0.001
$\delta F_{B\omega i}$	10^{-6}	8×10^{-7}	4×10^{-7}	2×10^{-7}	4×10^{-7}	3×10^{-7}
$\delta F_{B\Delta\omega i}$	0.027	0.008	0.011	0.009	0.014	0.007
δF_{Bi}	0.027	0.008	0.011	0.009	0.014	0.007
δT_{Di}/μs)	0.21	0.03	0.34	0.05	0.07	0.08
$\lvert\partial n_i/\partial T_{Di}\rvert$/ppm μs^{-1}	393216.1	1932815.9	1558195.7	11522535.9	2683562.3	1532906.2
$\lvert\partial n_i/\partial F_{Bi}\rvert$/ppm	1.72	3.18	8.82	120.16	4.50	13.30
δn_i/ppm	0.083	0.061	0.53	0.576	0.190	0.124

and the resulting error in determining concentration turned out to be 1.4 ppm.

Acknowledgements. This work was supported by the Russian Foundation for Basic Research (Grant No. 20-32-90025 Aspiranty) in the part concerning the development of the method for measuring the C-centre concentration in diamond and by the Russian Science Foundation (Grant No. 21-42-04407) in the part concerning the development of spectroscopy of spin bath in diamond and its coherent control.

References

1. Doherty M.W., Dolde F., Fedder H., Jelezko F., Wrachtrup J., Manson N.B., Hollenberg L.C.L. *Phys. Rev. B: Condens. Matter Mater. Phys.*, **85**, 1 (2012).
2. Simpson D.A., Ryan R.G., Hall L.T., Panchenko E., Drew S.C., Petrou S., Donnelly P.S., Mulvaney P., Hollenberg L.C.L. *Nat. Commun.*, **8**, 458 (2017).
3. Fang K., Acosta V.M., Santori C., Huang Z., Itoh K.M., Watanabe H., Shikata S., Beausoleil R.G. *Phys. Rev. Lett.*, **110**, 130802 (2013).
4. Kucsko G., Maurer P.C., Yao N.Y., Kubo M., Noh H.J., Lo P.K., Park H., Lukin M.D. *Nature*, **500**, 54 (2013).
5. Acosta V.M., Budker D., Hemmer P.R., Maze J.R., Walsworth R.L. *Opt. Magnetometry*, **8**, 142 (2011).
6. Steinert S., Ziem F., Hall L.T., Zappe A., Schweikert M., Götz N., Aird A., Balasubramanian G., Hollenberg L., Wrachtrup J. *Nat. Commun.*, **4**, 1607 (2013).
7. Rubinas O.R., Vorobyov V.V., Soshenko V.V., Bolshedvorskii S.V., Sorokin V.N., Smolyaninov A.N., Vins V.G., Yelisseyev A.P., Akimov A.V. *J. Phys. Commun.*, **2**, 115003 (2018).
8. Yelisseyev A., Babich Y., Nadolinny V., Fisher D., Feigelson B. *Diamond Relat. Mater.*, **11**, 22 (2002).
9. Dobrinets I.A., Vins V.G., Zaitsev A.M. *HPHT-Treated Diamonds* (Berlin–Heidelberg: Springer-Verlag, 2013).
10. Ajoy A., Bissbort U., Lukin M.D., Walsworth R.L., Cappellaro P. *Phys. Rev. X*, **5**, 011001 (2015).
11. Childress L.I. PhD Thesis (Cambridge: Harvard Uiversity, 2007).
12. Hahn E.L. *Phys. Rev.*, **80**, 580 (1950).
13. De Lange G., van der Sar T., Blok M., Wang Z.-H., Dobrovitski V., Hanson R. *Sci. Rep.*, **2**, 382 (2012).
14. Bauch E., Hart C.A., Schloss J.M., Turner M.J., Barry J.F., Kehayias P., Singh S., Walsworth R.L. *Phys. Rev. X*, **8**, 031025 (2018).
15. Xing J., Chang Y.C., Wang N., Liu G.Q., Pan X.Y. *Chin. Phys. Lett.*, **33** (10), 107601 (2016).
16. Wolf T., Neumann P., Isoya J., Wrachtrup J. *Phys. Rev. X*, **5**, 041001 (2014).
17. Rubinas O.R., Soshenko V.V., Bolshedvorskii S.V., Zeleneev A.I., Galkin A.S., Tarelkin S.A., Troschiev S.Y., Vorobyov V.V., Sorokin V.N., Sukhanov A.A., Vins V.G., Smolyaninov A.N., Akimov A.V. *Results Phys.*, **21**, 103845 (2021).
18. Acosta V.M., Bauch E., Ledbetter M.P., Santori C., Fu K.M.C., Barclay P.E., Beausoleil R.G., Linget H., Roch J.F., Treussart F., Chemerisov S., Gawlik W., Budker D. *Phys. Rev. B: Condens. Matter Mater. Phys.*, **80**, 1 (2009).
19. Stoneham A.M. *Mater. Sci. Eng. B*, **11**, 211 (1992).
20. Schweiger A., Jeschke G. *Principles of Pulse Electron Paramagnetic Resonance* (Oxford University Press, 2001).